WELDING RESEARCH

SUPPLEMENT TO THE *WELDING JOURNAL*, JUNE 2008
Sponsored by the American Welding Society and the Welding Research Council

Effect of GMAW Process and Material Conditions on DP 780 and TRIP 780 Welds

The effects of variables on microstructure and mechanical properties were explored for advanced high-strength steels

BY N. KAPUSTKA, C. CONRARDY, S. BABU, AND C. ALBRIGHT

ABSTRACT. The drive to reduce vehicle weight and improve crash performance has led automotive manufacturers to introduce higher-strength grades of advanced high-strength steels (AHSS). For these materials to be used effectively, the influence of material and process conditions on gas metal arc (GMA) weld properties must be understood. The objective of this work was to characterize the effects of material prestrain, cooling rate conditions (welding heat input and fixture heat sink), filler metal selection, dilution, and postbaking on the microstructure and mechanical properties of GMA welds on coated dual-phase (DP) and transformation-induced plasticity (TRIP) steels. The primary materials studied were DP 780 and TRIP 780; for comparison purposes a limited amount of work was conducted with DP 980. The DP steels showed varying degrees of heat-affected zone (HAZ) hardening and softening depending on the material grade, prestrain, and cooling rate condition. The relatively high aluminum content of the TRIP 780 allowed retained ferrite to be present in all regions of the HAZ, along with a continuous region of coarse ferrite along the weld interface. This resulted in the TRIP 780 having lower peak HAZ hardness than the DP 780. Fusion zone microstructure and hardness were found to be affected by the base metal chemistry, the cooling rate condition, and the filler metal composition. Filler metal strength did not affect the static or dynamic tensile properties of either the TRIP 780 lap or butt joint welds, or the DP 780 butt joint welds. All of the TRIP 780 and DP 780 butt joints failed in the soft HAZ. The results of the lap joint tests showed a greater variation in strength that is attributed to porosity at the root of the weld.

N. KAPUSTKA, C. CONRARDY, and S. BABU are with Edison Welding Institute, Columbus, Ohio. C. ALBRIGHT is with The Ohio State University, Columbus, Ohio.

Introduction

The use of AHSS has increased as a means of reducing vehicle weight through the use of thinner material gauges (Ref. 1). Future applications will likely require coated DP and TRIP steels with thicknesses of less than 2.0 mm (0.08 in.) and strength levels greater than 700 MPa (101.5 ksi). Gas metal arc welding (GMAW) is often employed where part geometry prevents the use of resistance spot welding (RSW) or when the design requires additional joint strength and stiffness.

To use AHSS effectively, it is important for designers and manufacturing engineers to understand the factors that may affect the performance of GMA-welded structures. This paper primarily explores the effects of common manufacturing variations on the microstructure and mechanical properties of coated DP 780 and TRIP 780. The effects of the following manufacturing variations were evaluated:

• **Material Prestrain**. Various degrees of strain may be imparted in the sheet metal during stamping or forming operations prior to welding.

• **Filler Metal Type**. Mild steel sheet applications typically employ common electrode compositions (e.g., ER70S) that are designed to produce weld metal having an ultimate tensile strength of at least 70 ksi (483 MPa). Higher-strength grades may be required to weld some AHSS grades in order to match the strength of the base metal.

• **Cooling Rate Conditions**. Weld cooling rates can be affected by the welding process parameters (i.e., welding heat input) as well as heat sinking from tooling or other adjacent materials.

• **Dilution**. Depending on the joint design and welding process parameters, the weld fusion zone alloy can consist of different fractions of base metal and filler metal.

• **Postbaking**. Components may be painted and baked after welding.

This work allows the relative importance of these factors on the weld microstructure and properties of DP 780 and TRIP 780 to be assessed. A limited amount of work was conducted with coated DP 980; the results of which are listed in table format for comparison purposes.

KEYWORDS

AHSS
Cooling Rate
DP Steels
Filler Metal
GMAW
Gas Metal Arc
TRIP Steels

Experimental Approach

Mechanized GMA welds were produced on coated steels under a range of conditions, including:

• **Material Grades**. Table 1 is a list of the steel grades that were evaluated, along with the nominal gauge thickness and coating type of each. Table 2 lists the chemical composition of each steel. The chemical compositions of the DP 780 and TRIP 780 steels were determined by inductively coupled plasma (ICP) analysis,

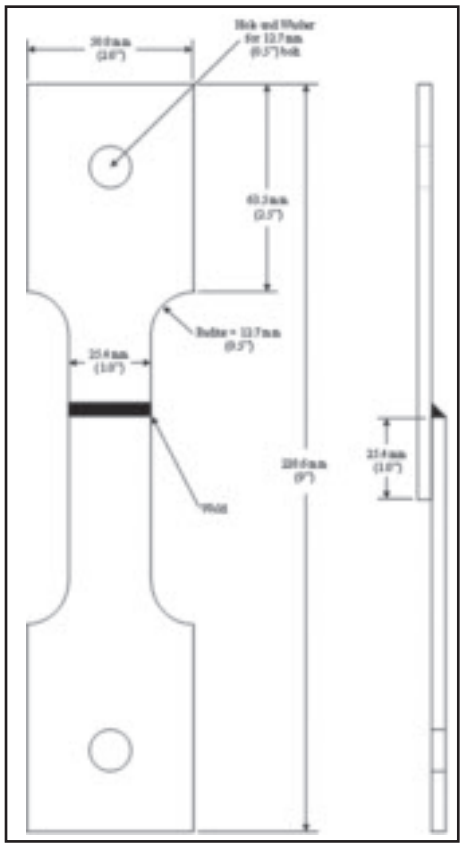

Fig. 1 — Reduced cross-sectional geometry of lap joint tensile specimens.

Table 1 — Base Materials Investigated

Grade	Coating	Thickness (mm)
DP 780	HDGA	1.54
DP 980	HDGA	1.60
TRIP 780	HDGA	1.35

Note: HDGA = Hot-dipped galvanized and annealed.

Table 2 — Base Metal Compositions

Element	TRIP 780	DP 780	DP 980
Carbon	0.17	0.13	0.112
Manganese	2.08	2.01	2.45
Silicon	0.023	<0.005	0.028
Phosphorous	0.011	0.016	0.013
Sulfur	<0.001	0.002	0.004
Copper	0.034	0.026	0.02
Nickel	0.021	0.015	0.01
Molybdenum	0.055	0.20	0.325
Chromium	0.094	0.23	0.24
Niobium	<0.001	<0.001	0.004
Vanadium	0.002	0.003	0.001
Titanium	0.010	0.002	0.003
Boron	<0.001	<0.001	0.0001
Aluminum	1.81	0.049	0.052
Nitrogen	0.0060	0.0096	—
Oxygen	0.0033	0.0078	—
Lead	<0.001	<0.001	—
Tungsten	0.002	<0.001	—
Zirconium	0.003	<0.001	—

Table 3 — Typical Welding and Heat Sink Conditions for Welds with Nominally High and Low Cooling Rates

Grade	Nominal Cooling Rate	Transfer Mode	Average Current (A)	Average Voltage (V)	Travel Speed (in./min)	Heat Sink	Heat Input (kJ/mm)
DP 780	High	SC	48.7	17.2	11.9	Copper	0.18
TRIP 780	High	SC	45	19.8	13.2	Copper	0.16
DP 780	Low	Spray	230	24.4	32	Air	0.40
TRIP 780	Low	Spray	237	24.8	45.1	Air	0.29

Table 4 — Test Matrix of Lap Welds for HAZ Characterization

Grade	Nominal Cooling Rate	Transfer Mode	Heat Sink	Heat Input (kJ/mm)
DP 780	High	SC	Copper	0.17
DP 780	Low	Spray	Air	0.41
TRIP 780	High	SC	Copper	0.16
TRIP 780	Low	Spray	Air	0.29

Note: Test matrix repeated for prestrained coupons.

while the composition of the DP 980 steel is that which was provided in the manufacturer's certification.

• **Joint Types**. Lap joint fillet welds were produced for HAZ characterization. Both lap joint fillet welds and square groove butt joint welds were produced for fusion zone and mechanical property characterization. As shown in Fig. 1, the lap joints had 25.4 mm (1.0 in.) of overlap. Lap joints were produced using 140- × 203-mm (5½- × 8-in.) coupons, while butt joints used 127- × 203-mm (5- × 8-in.) coupons.

• **Prestrain**. Two conditions were used: as-received and prestrained via roll reduction in thickness of approximately 8%.

• **Filler Metal**. Two filler metals were used: a nominally "low"-strength electrode (ER70S-6) and a nominally "high"-strength electrode (ER100S-G).

• **Heat Sink Effects**. Welds were produced at nominally high and low cooling rate conditions. High cooling rate was achieved with short-circuit transfer and a copper backing bar. Low cooling rate was achieved with spray transfer and no backing bar. Table 3 lists typical welding parameters and heat sink conditions used to produce welds with a nominally high or low cooling rate. Parameters were developed to achieve adequate fusion without excessive penetration (i.e., no melt-through on lap joints). For butt joint welds, the major acceptance criteria was full penetration, without excessive root reinforcement. The fixture (Fig. 2) had a ½-in.-deep × 1-in.-wide channel along the weld centerline. A copper bar was inserted into the channel for the high heat sink welds. For the no heat sink welds, the copper bar was removed. A computerized data acquisition system was employed to measure the current, voltage, and time of each weld; travel speeds were determined by dividing the weld length by the weld time. The average theoretical heat input of each weld was calculated to provide an indication of the actual heat input. Because heat input calculations were determined for comparative purposes, a heat transfer efficiency of 1.0 was used.

Table 5 — Gleeble Test Conditions for HAZ Characterization

Sample	Peak Temperature (°C)	Heating Rate (°C/s)
1	500	25
2	1000	25
3	1000	0.16

• **Postbake**. Samples were evaluated

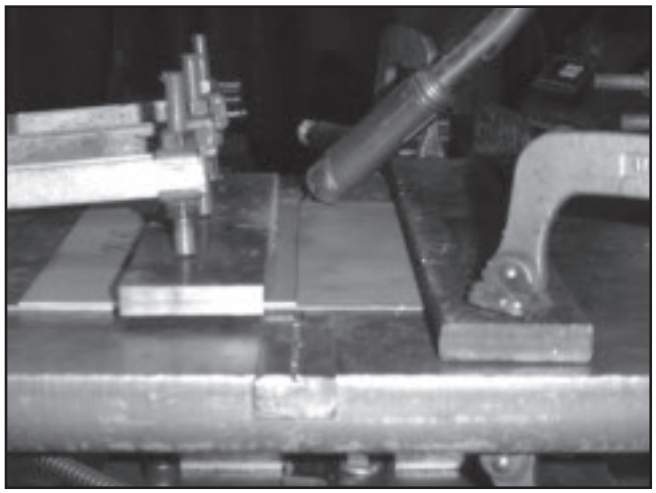

Fig. 2 — Fixture used to produce different heat sink conditions.

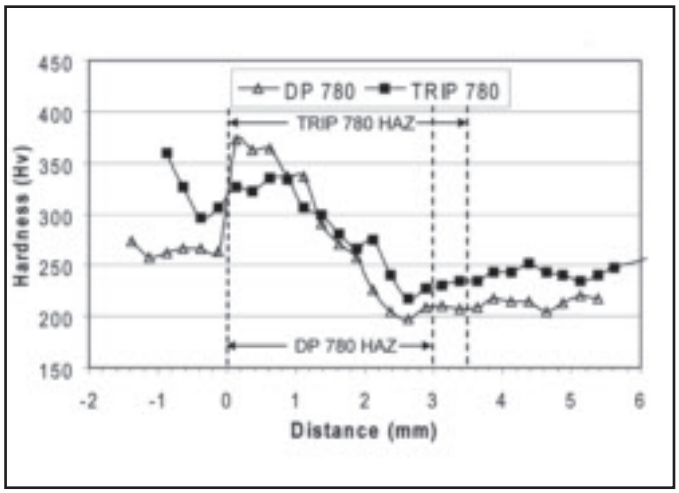

Fig. 3 — Hardness profiles of DP 780 and TRIP 780 lap welds produced with the nominally high cooling rate: no prestrain or postbaking.

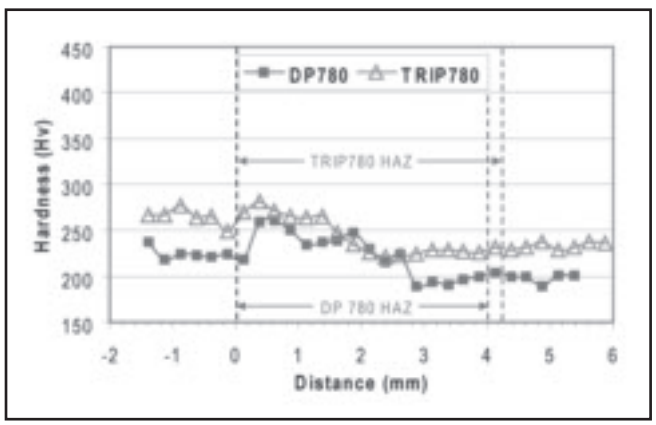

Fig. 4 — Hardness profiles of DP 780 and TRIP 780 lap welds produced with the nominally low cooling rate: no prestrain or postbaking.

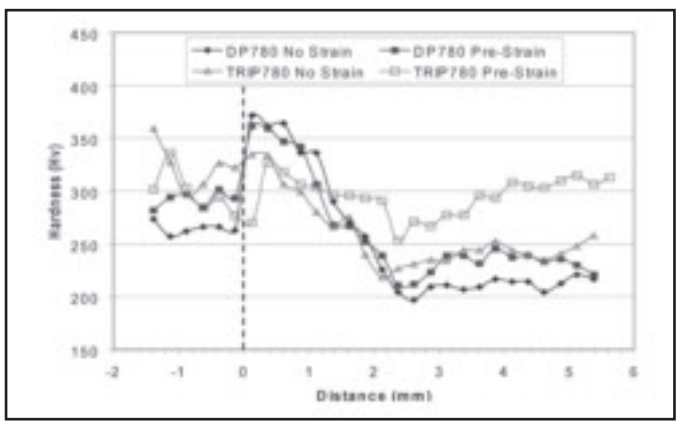

Fig. 5 — Hardness profiles of DP 780 and TRIP 780 lap welds produced both with and without prestrain for the high cooling rate condition.

both with and without postbaking. Postbaking consisted of placing welded specimens in a preheated oven, allowing the specimens to heat, holding the specimens at 170°C for 25 min., then removing from the oven and allowing to air cool.

The HAZ and fusion zone hardness profiles and microstructures of the GMA welds were characterized. Static and dynamic tensile properties of DP 780 and TRIP 780 were also evaluated and related to the microstructural observations. The weld evaluation approach is described below in three parts.

HAZ Characterization

The effects of grade, prestrain, cooling rate condition, and postbake on the HAZ microstructure and hardness profile were evaluated. Lap welds for HAZ evaluation were produced using ER70S-6 wire. Table 4 is the test matrix, which was applied for the lap joints both with and without prestrain. To ensure that steady-state conditions had been reached, metallographic cross sections were taken at least 3 in. from the start of the weld. One cross section was examined in the as-received condition, while another underwent a postbake treatment prior to metallographic preparation. Hardness traverses were taken along the centerline of the top sheet.

Gleeble testing was performed to relate the phase transformations that occur at different HAZ locations to the temperature at which the location was heated. Table 5 is the test matrix used during the Gleeble trials. 5- × 75-mm (0.020- × 2.95-in.) samples were heated at the rates listed and then cooled to room temperature at approximately 40°C/s. Each sample was

Table 6 — Test Matrix of Lap Welds for Fusion Zone Characterization

Steel Grade	Filler Metal	Nominal Cooling Rate	Transfer Mode	Heat Sink	Heat Input (kJ/mm)
DP 780	ER70S-6	High	SC	Copper	0.15
DP 780	ER70S-6	Low	Spray	Air	0.43
DP 780	ER100S-G	High	SC	Copper	0.19
DP 780	ER100S-G	Low	Spray	Air	0.41
TRIP 780	ER70S-6	High	SC	Copper	0.16
TRIP 780	ER70S-6	Low	Spray	Air	0.34
TRIP 780	ER100S-G	High	SC	Copper	0.19
TRIP 780	ER100S-G	Low	Spray	Air	0.29

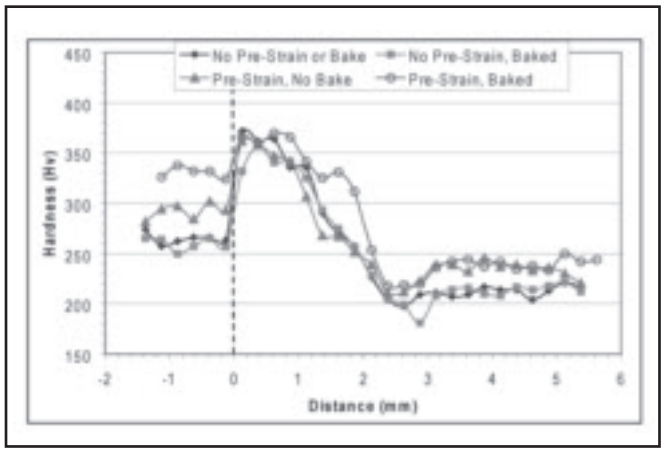

Fig. 6 — Hardness profiles of DP 780 lap welds with and without postbaking for both prestrained and not prestrained sheet. (Welds were produced with the nominally high cooling rate condition.)

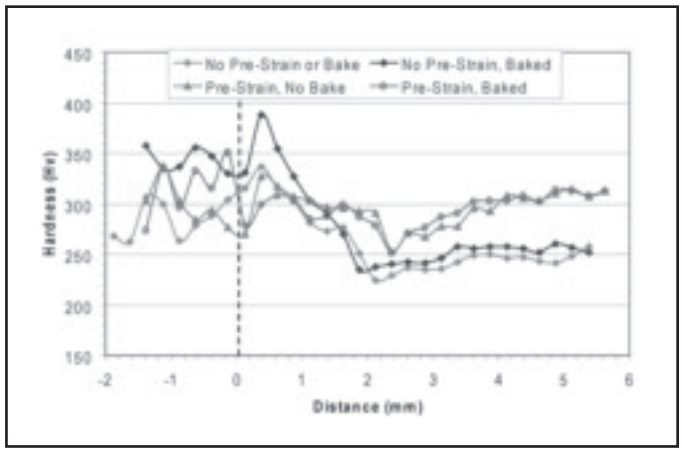

Fig. 7 — Hardness profiles of TRIP 780 lap welds with and without postbaking for both prestrained and not prestrained sheet. (Welds were produced with the nominally high cooling rate condition.)

then cross sectioned along its center (the location where the temperature reached that listed in Table 5) and prepared for metallographic examination and hardness testing.

Fusion Zone Characterization

The effects of filler metal selection, cooling rate condition, and dilution on the fusion zone microstructure and hardness were evaluated. The test matrices of the lap and butt joints are shown in Tables 6 and 7, respectively. DP 780 and TRIP 780 lap and butt joints were produced using both ER70S-6 and ER100S-G wire types. To ensure that steady-state conditions had been reached, metallographic cross sections were taken at least 3 in. from the start of the weld. For each specimen dilution of the filler metal by the base metal was approximated from the macrographs using imaging software. In addition, the weld metal chemistry of the high and low cooling rate TRIP 780 lap welds produced with the ER70S-6 wire was analyzed to verify the dilution estimates.

Table 7 — Test Matrix of Butt Joint Welds for Fusion Zone Characterization

Steel Grade	Filler Metal	Nominal Cooling Rate	Transfer Mode	Heat Sink	Heat Input (kJ/mm)
DP 780	ER70S-6	High	SC	Copper	0.20
DP 780	ER70S-6	Low	Spray	Air	0.17
DP 780	ER70S-6	High	SC	Copper	0.17
DP 780	ER70S-6	Low	Spray	Air	0.18
TRIP 780	ER70S-6	High	SC	Copper	0.20
TRIP 780	ER70S-6	Low	Spray	Air	0.18
TRIP 780	ER100S-G	High	SC	Copper	0.19
TRIP 780	ER100S-G	Low	Spray	Air	0.18

Table 8 — Test Matrix of Lap and Butt Joint Welds for Mechanical Property Characterization

Steel Grade	Filler Metal	Nominal Cooling Rate	Transfer Mode	Heat Sink	Joint Geometry	HI (kJ/mm)
DP 780	ER70S-6	High	SC	Copper	Butt	0.20
DP 780	ER70S-6	Low	Spray	Air	Butt	0.17
DP 780	ER100S-G	High	SC	Copper	Butt	0.17
DP 780	ER100S-G	Low	Spray	Air	Butt	0.18
TRIP 780	ER70S-6	High	SC	Copper	Lap	0.16
TRIP 780	ER70S-6	Low	Spray	Air	Lap	0.29
TRIP 780	ER100S-G	High	SC	Copper	Lap	0.18
TRIP 780	ER100S-G	Low	Spray	Air	Lap	0.29
TRIP 780	ER70S-6	High	SC	Copper	Butt	0.20
TRIP 780	ER70S-6	Low	Spray	Air	Butt	0.18
TRIP 780	ER100S-G	High	SC	Copper	Butt	0.19
TRIP 780	ER100S-G	Low	Spray	Air	Butt	0.18

Mechanical Property Characterization of DP 780 and TRIP 780

The static and dynamic tensile strength of lap and butt joints produced using TRIP 780, and butt joints produced using DP 780 were assessed. Table 8 is the welding matrix used in producing the mechanical test specimens. To achieve complete penetration and avoid melt-through, the calculated welding heat input of all butt joint welds was similar. Thus, cooling rate was affected primarily by the heat sink condition for the butt joint welds. For the TRIP 780 lap joints, a broader range of calculated welding heat input levels were used in combination with heat sinking to affect cooling rate.

For each welding condition listed in Table 8, three specimens underwent static tensile testing and three specimens underwent dynamic tensile testing. Weld metal reinforcement was machined from the surface of the butt joint welds so that the fusion zone thickness was similar to that of the base material. Coolant was used during machining to minimize metallurgical effects. All specimens were laser cut into the reduced cross-sectional geometry shown in Fig. 1. The butt and lap joint tensile specimens were similar; with the primary difference being the location of the weld. For the butt joints, the weld was in the middle of the specimen, while for the lap joints the overlapped region was in the middle of the specimen. To avoid slippage, 12.5-mm- (½-in.-) diameter holes were first placed 25 mm (1 in.) from the end of each specimen. These holes were then reinforced with 12.5-mm-diameter washers that were spot welded to the specimen. To minimize bending on the lap joint tensile

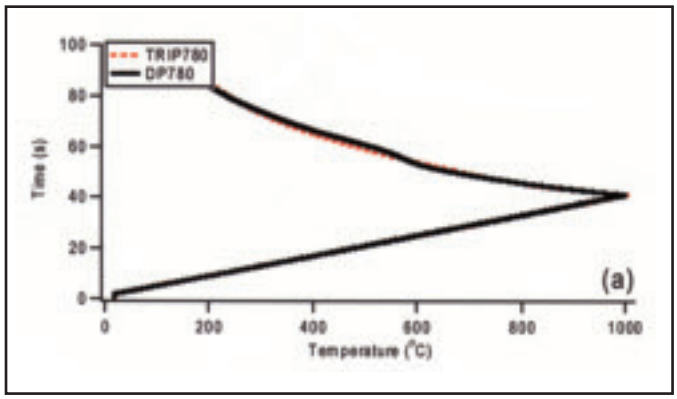

Fig. 8 — Comparison of measured temperature cycle from DP 780 and TRIP 780 steels during heating and cooling to 1000°C at 25°C/s. [It is important to note during cooling cycle no forced cooling was used to track the heat of transformation from austenite to ferrite. The DP 780 steels showed significant change in cooling rate as the transformation starts at ~600°C (solid arrow). No such change in cooling rate was observed in TRIP 780 steels.]

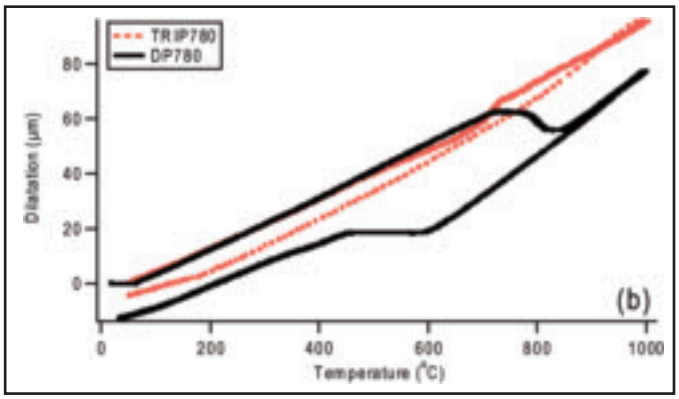

Fig. 9 — Measured dilation corresponding to the temperature cycle shown in Fig. 8. [DP 780 steel shows classical behavior: on heating austenite formation above 700°C and on cooling transformation from austenite to ferrite below 600°C (marked by solid arrow). It is interesting to note that the TRIP 780 steels show a small change in dilation on heating above 500°C and then no classical austenite to ferrite transformation.]

specimens, 12.5-mm-thick plates were placed on the surface opposite the washers during testing.

The static tensile specimens were tested at a rate of 50 mm/min (2.0 in./min). The dynamic tensile specimens were tested using two different weights and a constant drop height of 10 ft. Initially, a 58.5-lb weight was used. When it was realized that this weight was inadequate to break all specimens, a 106.7-lb weight was used. Analysis of the peak load vs. strain at peak load, and the peak load vs. elongation at peak load curves indicated that the different weights did not have a significant effect on dynamic tensile properties. For all tensile tests, peak load, energy at peak load, and elongation at peak load were recorded.

Results

The results of the HAZ characterization, fusion zone characterization, and mechanical property characterization are presented separately. The Discussion section of this paper then relates these results.

HAZ Characterization

Figures 3–6 show hardness profiles for welds made on DP 780 and TRIP 780 using ER70S-6 wire under a range of heat sink and prestrain conditions. The zero on the X-axis represents the fusion boundary location with HAZ to the right and fusion zone to the left. Note that the HAZ boundary was defined as the location in which the hardness in the HAZ reaches the average hardness of the base metal. The data presented in these figures are summarized in Table 9; data for DP 980 lap welds produced with ER70S-6 welding wire are also listed. Referring to Table 9, ΔH_{Pk} and ΔH_{Min} are the degrees of HAZ hardening and softening, respectively. The figures show various degrees of HAZ hardening and softening depending on material grade and other conditions. The highest hardness occurs in the near HAZ (adjacent to the fusion boundary), while the softest point is in the far HAZ. Compared to TRIP 780, DP 780 has a higher degree of hardening and a slightly lower degree of softening. The following provides additional description of the results in these figures:

• **Cooling Rate**. Figure 3 shows hardness profiles for welds produced with the nominally high cooling rate condition (i.e., combination of low heat input and heat sink). Figure 4 shows hardness profiles for

Table 9 — HAZ Characterization Data for Lap Welds Produced on DP 780, TRIP 780, and DP 980 Using ER70S-6 Welding Wire

	Condition			H_{Pk}	ΔH_{Pk}	H_{Min}	ΔH_{Min}	Width
Grade	Cooling Rate	Prestrain	Baking	(Hv)	(%)	(Hv)	(%)	(mm)
DP 780	High	No	No	372	80	197	–5	3.0
	Low	No	No	261	26	189	–9	4.0
	High	Yes	No	362	52	211	–11	3.2
	Low	Yes	No	294	24	207	–13	4.5
	High	No	Yes	357	72	181	–13	3.0
	Low	No	Yes	280	35	187	–10	4.0
	High	Yes	Yes	370	55	218	–8	3.2
	Low	Yes	Yes	311	31	210	–12	4.8
TRIP 780	High	No	No	334	34	218	–8	3.8
	Low	No	No	277	11	211	–11	4.2
	High	Yes	No	327	5	253	–18	4.2
	Low	Yes	No	282	–9	261	–16	5.0
	High	No	Yes	388	55	235	–6	3.5
	Low	No	Yes	302	21	220	–12	4.2
	High	Yes	Yes	308	–1	252	–19	4.2
	Low	Yes	Yes	300	–3	259	–16	5.0
DP 980	High	No	No	392	28	266	–13	3.5
	Low	No	No	344	12	250	–18	5.2
	High	Yes	No	402	15	274	–22	NA
	Low	Yes	No	381	9	252	–28	NA
	High	No	Yes	407	27	270	–16	3.2
	Low	No	Yes	362	17	258	–17	5.4
	High	Yes	Yes	400	14	291	–17	NA
	Low	Yes	Yes	383	9	284	–19	NA

H_{Pk} = Peak HAZ hardness — $\Delta H_{Pk} = [(H_{Pk} - \text{Base Metal Hardness}) - 1] \times 100$

H_{Min} = Minimum HAZ hardness — $\Delta H_{Min} = [(H_{Min} - \text{Base Metal Hardness}) - 1] \times 100$

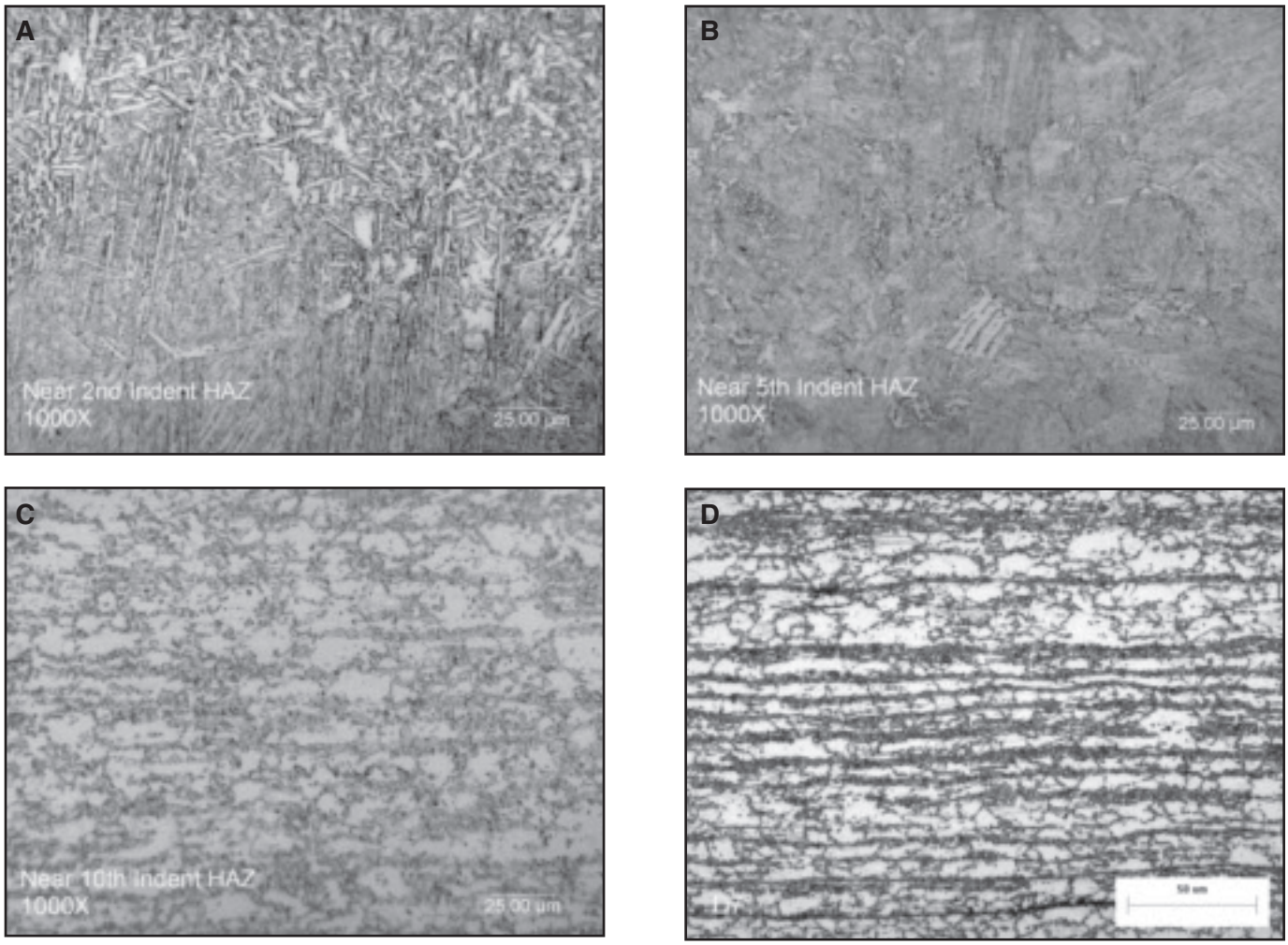

Fig. 10 — Micrographs of the DP 780 HAZ and base metal for a lap weld produced with the nominally high cooling rate condition (2% Nital etch). A — 2nd indent in HAZ (370 HV, 1000×); B — 5th indent in HAZ (340 HV, 1000×); C — 10th indent in HAZ (195 HV, 1000×); D — base metal (207 HV, 500×).

the DP 780 and TRIP 780 welded with the nominally low cooling rate (i.e., combination of high heat input and no heat sink). The plots show that cooling rate tends to have the largest effect on the DP steel, with the TRIP steel being somewhat less affected. Lower cooling rates tend to produce a wider HAZ (as identified from the hardness profile) with lower peak hardness. For example, the DP 780 peak hardness was about 80% higher than the base metal for the high cooling rate condition, and about 25% higher than the base metal for the low cooling rate condition. The lower cooling rate also tends to produce slightly more HAZ softening. The TRIP 780 showed about 11% reduction in hardness compared to the base metal.

• **Material Prestrain**. Figure 5 shows hardness profiles for DP 780 and TRIP 780 welds made both with and without prestrain for the high cooling rate condition. Prestrain has the largest effect on the TRIP base material, increasing the base metal hardness by about 25%. The hardness of the softest location of the TRIP 780 HAZ is also increased by prestrain; with the degree of softening being slightly increased (about 3–10%). The softest point in the TRIP 780 HAZ remains greater than the hardness of the as-received base metal. Prestraining increased the DP 780 base metal hardness by only about 10%. Prestraining did not affect the peak HAZ hardness for either material.

• **Postbake**. Figure 6 shows hardness profiles of DP 780 welds with and without postbaking for both prestrained and not prestrained sheet. Based on these data, postbaking did not appear to have a significant influence on the HAZ hardness profiles of the DP 780 material, regardless of prestrain condition. Figure 7 shows a

Table 10 — Fusion Zone Microstructure, Hardness, and Dilution of DP 780 Welds Produced with ER70S-6 Electrode

Heat Input (kJ/mm)	Nominal Cooling Rate	Heat Sink	Dilution (%)	Average Hardness	Microstructure
				Lap Welds	
0.15	High	Copper	21	269	Predominately AF with a small fraction of B
0.43	Low	Air	59	251	Predominately AF with a small fraction of B
				Butt Joint Welds	
0.20	High	Copper	46	309	Predominately AF with some B and M (very fine microstructure)
0.17	Low	Air	52	266	Mixture of B and AF

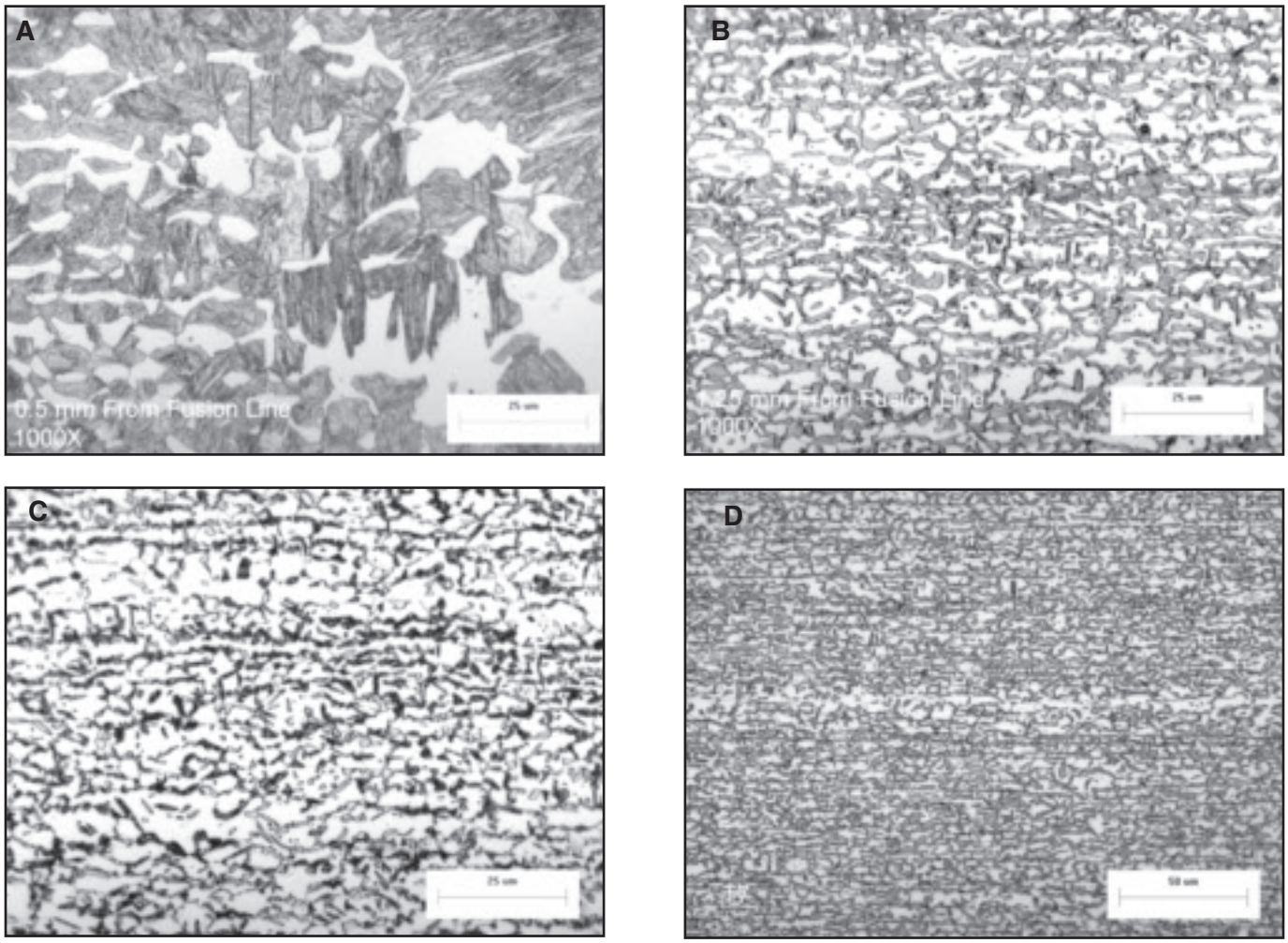

Fig. 11 — Micrographs of the TRIP 780 HAZ and base metal for a lap weld produced with the nominally high cooling rate condition (2% Nital etch). A — 2nd indent in HAZ (335 HV, 1000×); B — 5th indent in HAZ (275 HV, 1000×); C — 10th indent in HAZ (224 HV, 1000×); D — base metal (254 HV, 500×).

similar result for the TRIP 780 material.

Referring to Table 9, comparison of these two steels with DP 980 indicates that although DP 980 had the highest peak HAZ hardness, DP 780 had the highest degree of HAZ hardening. Furthermore, the DP 980 generally had a higher degree of HAZ softening compared to the DP 780 and TRIP 780 materials.

Figures 8 and 9 show Gleeble test results for the DP 780, and TRIP 780 steel heated to 1000°C at 25°C/s. Figure 8 is a plot of measured thermal cycles during heating and cooling of these steels. It is noteworthy that during these experiments, the heating rates were controlled precisely and the cooling rate was allowed to be modified by heat of transformation. The plots clearly show an abrupt change in the cooling curve slope (marked by arrow) for the DP 780 steels. Figure 9 shows the corresponding measured dilatation for the same samples. In DP 780, specimen expansion is nearly linear with increased temperature within the ranges of room temperature to 720°C and 860° to 1000°C. Upon heating through the temperature range of 720° to 860°C, the specimen width decreases and then begins to once again increase. This, along with the fact that the linear coefficient of thermal expansion (CTE) is lower in the range of 100° to 720°C than from 860° to 1000°C, suggests that the initial microstructure transformed to austenite between 720° and 860°C. Similar heating curves were observed for the DP 980 specimens that underwent similar thermal cycles and will be presented in future work. The measured dilation curve for TRIP 780 is significantly different than that which was observed for the DP materials. Upon heating to

Table 11 — Fusion Zone Microstructure, Hardness, and Dilution of DP 780 Welds Produced with ER100S-G Electrode

Heat Input (kJ/mm)	Nominal Cooling Rate	Heat Sink	Dilution (%)	Average Hardness	Microstructure
			Lap Welds		
0.19	High	Copper	38	326	Mixture of M and B
0.41	Low	Air	53	274	Predominately AF with a small fraction of B
			Butt Joint Welds		
0.17	High	Copper	46	317	Predominately AF, which is probably interweaved with M. Some WF
0.18	Low	Air	54	307	Predominately AF with some areas of B

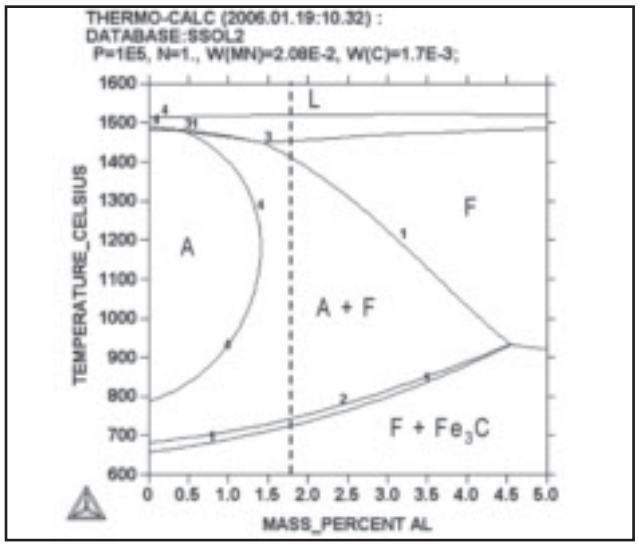

Fig. 12 — Equilibrium phase diagram of TRIP 780 calculated with Thermo-Calc™ software, chemical composition determined by ICP analysis.

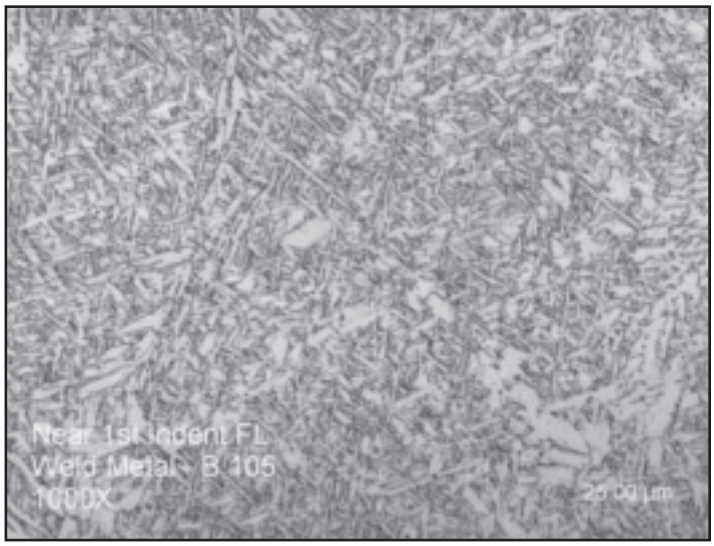

Fig. 13 — Weld metal microstructure of the DP 780/ER70S-6 lap weld produced at high cooling rate.

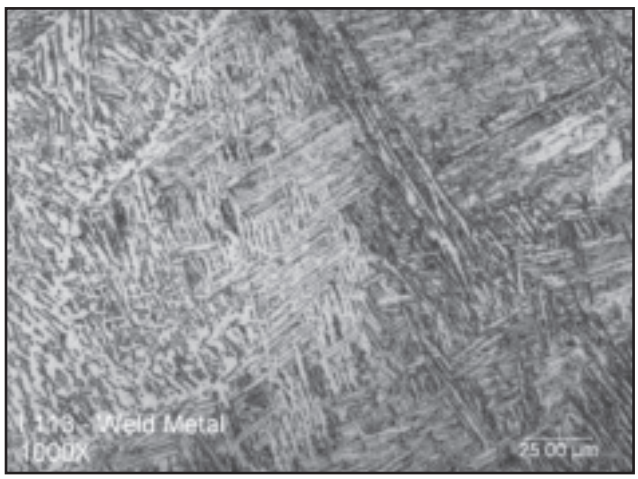

Fig. 14 — Weld metal microstructure of the TRIP 780/ER70S-6 lap weld produced at high cooling rate.

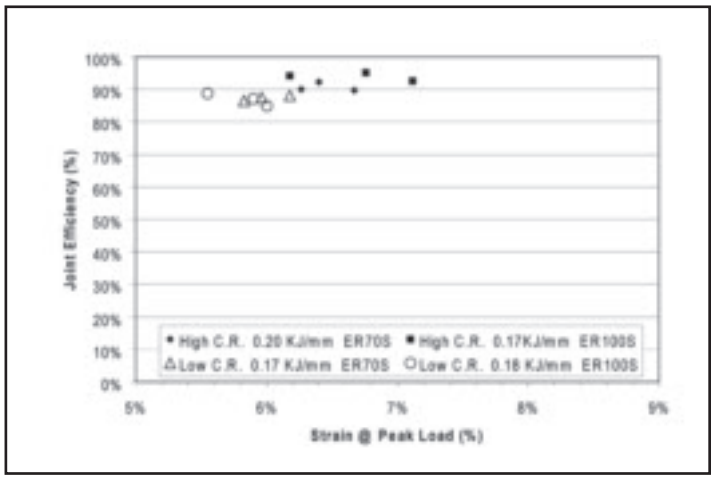

Fig. 15 — Static tensile test results of DP 780 butt joints.

1000°C, no large changes in the CTE were observed, which suggests that the TRIP 780 does not fully transform to austenite. The difference in transformation strains is attributed to increased ferrite stability in the TRIP 780. However, more work is necessary to understand these complex transformations at different heating and cooling rates.

To relate the hardness data to microstructures, micrographs were taken at various HAZ locations of the DP 780 and TRIP 780 welds. Figure 10 shows regions of the DP 780 HAZ and base metal of a high cooling rate weld. The top-left micrograph was taken near the location of peak HAZ hardness (370 HV). The bottom half of the image (where the hardness was measured) has a microstructure that consists of predominately martensite with some bainite. Moving farther away from the fusion boundary, the top-right micrograph shows a slightly softer (340 HV) region with a mixture of martensite and bainite. The bottom-left micrograph shown in Fig. 10 was taken near the minimum hardness (195 HV) location of the high cooling rate weld HAZ. As shown, the microstructure is indistinguishable from that of the base metal.

By comparison, the microstructure of the low cooling rate DP 780 weld (not shown) in the area of peak hardness (260 HV) consists of predominately bainite with some grain boundary ferrite. These data suggest that the significant increase in peak hardness in the high cooling rate weld near HAZ is due to the higher volume fraction of martensite.

Micrographs taken at various locations of the TRIP 780 high cooling rate weld HAZ are shown in Fig. 11. The top-left micrograph was taken near the point of peak HAZ hardness (335 HV) and has a microstructure that consists of a mixture of martensite and large ferrite grains. The top-right micrograph was taken farther from the fusion boundary in a softer HAZ region (275 HV) and has a mixture of large ferrite grains and degenerate martensite. Note that the term degenerate martensite is used to describe regions that appear to be martensite at optical microscopy levels, but may contain tempered martensite and/or bainite constituents (Ref. 2). Comparison of the top-left and top-right micrographs shown in Fig. 11 in-

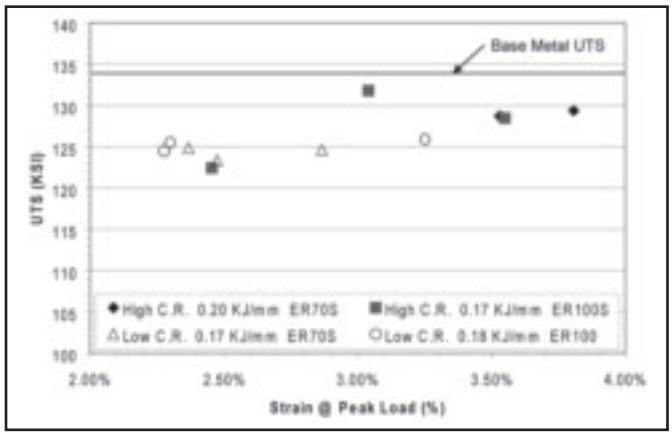

Fig. 16 — Dynamic tensile test results of DP 780 butt joints.

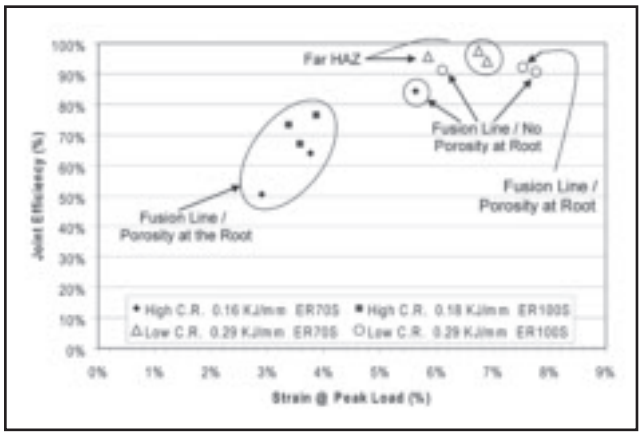

Fig. 17 — Static tensile test results of TRIP 780 lap joints.

dicates that the fraction of ferrite increases with distance from the point of peak HAZ hardness. The bottom-left micrograph is in the softened region and appears similar to that of the base metal, consisting of predominately ferrite with islands of degenerate martensite. The darker contrast of many of the degenerate martensite islands suggests tempering has occurred during the weld thermal cycle.

By comparison, the microstructure of the low cooling rate TRIP 780 weld HAZ (not shown) at the location of peak hardness (275 HV) consists predominately of ferrite grains separated by regions of a fine dispersion of degenerate martensite. Again, this suggests that the lower martensite content is responsible for the reduced peak hardness.

It should be noted that the weld interface of the TRIP 780 welds consists of a continuous band of ferrite grains. The ferrite grains are larger along the weld interface of the high cooling rate weld than along the weld interface of the low cooling rate weld. It was observed that for both cooling rate conditions the fraction of ferrite decreased from the weld interface to the location of peak HAZ hardness, and then increased as the point of minimum HAZ hardness was approached. Between the point of minimum HAZ hardness and the HAZ boundary (unaffected base metal), the area fraction of ferrite in the microstructure appears constant.

Additional analysis was done to better understand the TRIP 780 HAZ phase transformations. The composition of the TRIP 780 was determined by ICP analysis. The aluminum content was found to be 1.8%, which is about 1% higher than the nominal composition indicated by the manufacturer. Using this composition, the equilibrium phase diagram shown in Fig. 12 was determined using Thermo-Calc™ software (Ref. 3). As shown in Fig. 12, the TRIP 780 steel isn't expected to transform to 100% austenite on heating to higher temperature. In other words, ferrite is thermodynamically stable at all temperatures below the melting point with 1.8% aluminum. The phase diagram also shows that we would expect 100% austenite formation if the nominal composition of 0.8% aluminum was used.

Fusion Zone Characterization

Figures 3 and 4 show hardness profiles of DP 780 and TRIP 780 welded with ER70S-6 for the high and low cooling rate conditions, respectively. Tables 10–13 list the nominal cooling rate conditions, dilution, average hardness, and microstructure of DP 780 and TRIP 780 lap and butt joint welds produced with both the ER70S-6 and ER100S-G wires. For comparison purposes, similar data for DP 980 lap welds produced with ER70S-6 wire are listed in Table 14.

Figure 13 shows the weld metal microstructure of the DP 780/ER70S-6 lap weld produced with a high cooling rate, consisting predominately of acicular ferrite with a small fraction of bainite. As Table 10 indicates, lap joints produced at both high and low cooling rates had a similar microstructure, although the low cooling rate was found to have a somewhat softer and coarser microstructure. The butt joint welds produced with high cooling rate consisted of predominately acicular ferrite with some bainite and martensite. At low cooling rates the butt joint weld consisted of a mixture of acicular fer-

Table 12 — Fusion Zone Microstructure, Hardness, and Dilution of TRIP 780 Welds Produced with ER70S-6 Electrode

Heat Input (kJ/mm)	Nominal Cooling Rate	Heat Sink	Dilution (%)	Average Hardness	Microstructure
			Lap Welds		
0.16	High	Copper	37	271	Predominately B with a small fraction of AF
0.34	Low	Air	59	256	Predominately B with a small fraction of AF, (B has higher aspect ratio)
			Butt Joint Welds		
0.20	High	Copper	44	283	Predominately B, no AF
0.18	Low	Air	57	278	Predominately B with a small fraction of AF

Table 13 — Fusion Zone Microstructure, Hardness, and Dilution of TRIP 780 Welds Produced with ER100S-G Electrode

Heat Input (kJ/mm)	Nominal Cooling Rate	Heat Sink	Dilution (%)	Average Hardness	Microstructure
				Lap Welds	
0.19	High	Copper	31	369	Mixture of M and B
0.30	Low	Air	54	317	Predominately B with some AF
				Butt Joint Welds	
0.19	High	Copper	44	389	Most likely M
0.18	Low	Air	57	333	Predominately B with some M

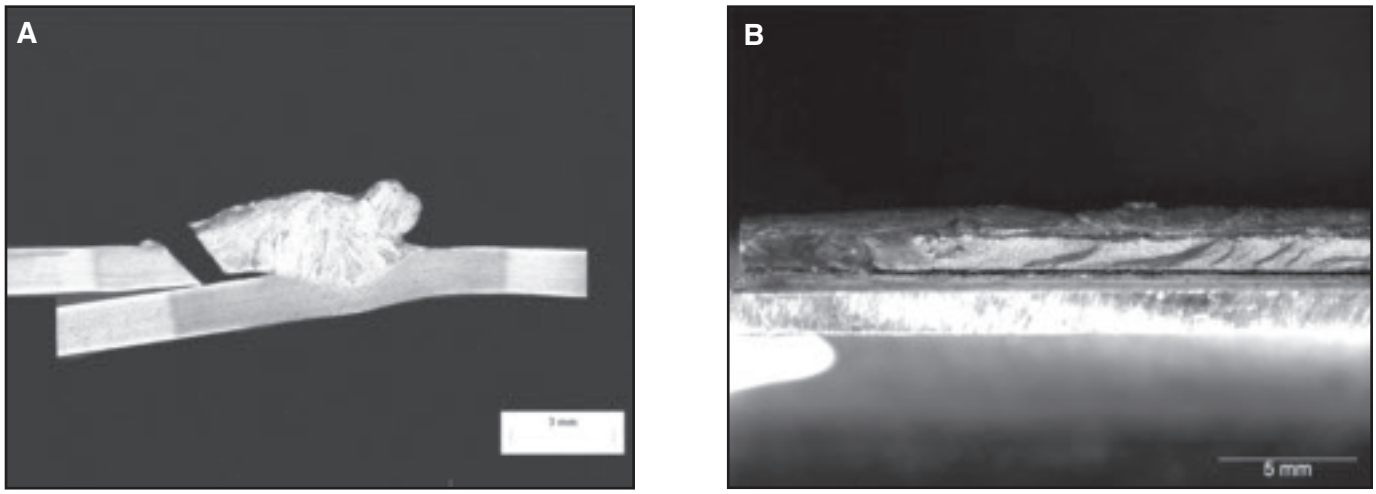

Fig. 18 — Fracture appearance of TRIP 780 low cooling rate lap joint produced with the ER100S-G wire. (Failure is along the weld interface of the top sheet.)

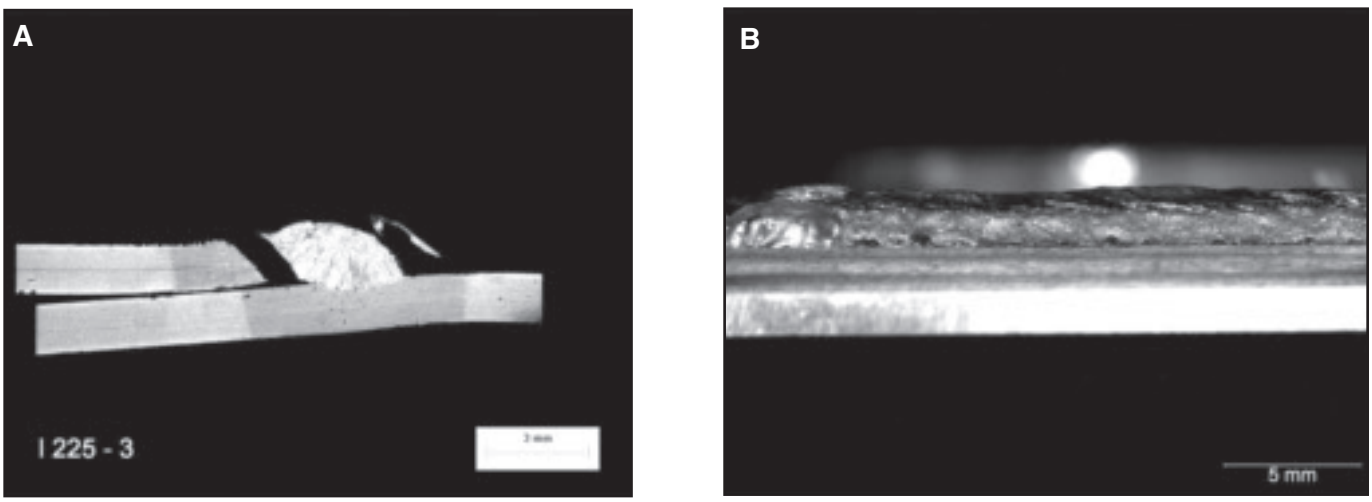

Fig. 19 — Fracture appearance of TRIP 780 high cooling rate lap joint produced with the ER100S-G wire. (Failure is along the weld interface of the top sheet, possibly initiating at porosity present at the root.)

Table 14 — Fusion Zone Microstructure, Hardness, and Dilution of DP 980 Lap Welds Produced with ER70S-6 Electrode

Heat Input (kJ/mm)	Nominal Cooling Rate	Heat Sink	Dilution (%)	Average Hardness	Microstructure
0.15	High	Copper	20	263	Predominately AF with a small fraction of B
0.44	Low	Air	59	253	Predominately AF with a small fraction of B

Table 15 — Carbon Equivalents, Aluminum, and Silicon Contents of Each Base Material

Material	CE	Aluminum (wt-%)	Silicon (wt%)
TRIP 780	0.53	1.81	0.023
DP 780	0.47	0.049	0.005
DP 980	0.49	0.052	0.028

Note: CE = C + A(C) * [Si/24 + Mn/6 + Cu/15 + Ni/20 + (Cr + Mo + Nb + V)/5 + 5*B]
A(C) = 0.75 + 0.25*tanh[20*(C – 0.12)]

rite and bainite. Table 11 indicates the cooling rate conditions and relates them to the average hardness, dilution, and microstructure of the DP 780 welds produced with the ER100S-G wire. The microstructure of the high cooling rate lap weld consisted of a mixture of martensite and bainite, while the low cooling rate lap weld consisted of predominately acicular ferrite with a small fraction of bainite. Butt joint welds were predominantly acicular ferrite with either martensite (for the high cooling rate welds) or bainite (for the low cooling rate welds). Thus, the fusion zone microstructure of the DP 780 was affected by filler metal type, joint design, dilution, and cooling rate.

Figure 14 shows the weld metal microstructure of the TRIP 780/ER70S-6 lap weld produced at a high cooling rate, consisting predominately of bainite with a small fraction of acicular ferrite. As Table 12 indicates, the fusion zone microstructure and hardness obtained for the TRIP 780 lap welds consists predominately of bainite with a small fraction of acicular ferrite. The microstructure of the butt joint welds consisted primarily of bainite, with the low cooling rate weld having a

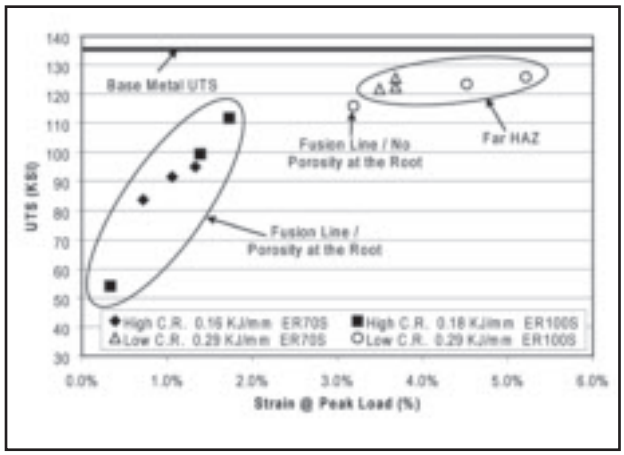

Fig. 20 — Dynamic tensile test results of TRIP 780 lap joints.

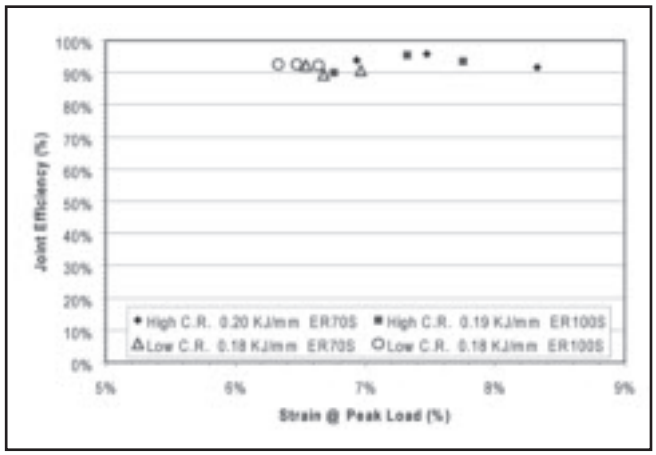

Fig. 21 — Static tensile test results of TRIP 780 butt joints.

small fraction of acicular ferrite. Table 13 lists the microstructure and hardness of the TRIP 780 welds produced with the ER100S-G wire. The fusion zone microstructure of the welds at high cooling rate consisted predominantly of martensite. These welds had significantly higher hardness than those produced at low cooling rate, which were predominantly bainite with some martensite or acicular ferrite.

Table 14 lists the microstructure, average hardness, and dilution of the DP 980 lap welds produced with a high and low cooling rate using ER70S-6 wire. The microstructure of both welds is primarily acicular ferrite with a small fraction of bainite. In this case, cooling rate did not have a large influence on microstructure or hardness. Referring to the HAZ characterization data listed in Table 9, the DP 980 weld fusion zone is softer than any point in the weld HAZ. This suggests that an undermatched strength condition may exist when DP 980 is welded with ER70S-6 wire. Depending on the loading condition, failure may be expected to occur through the softer weld metal. Comparing the fusion zone characterization data of the DP 780 and DP 980 lap joints (Table 10 and Table 14, respectively) indicates that the microstructures and hardness values obtained were very similar. Therefore, the base metal composition did not significantly affect the fusion zone microstructure for the DP steels.

Mechanical Property Characterization

The static tensile test results of the DP 780 butt joints are shown in Fig. 15. The results are expressed in terms of joint efficiency (i.e., weld ultimate tensile strength/measured base metal ultimate tensile strength) and the strain at peak load. All of these welds failed in the softened region of the far HAZ. As shown, the high cooling rate welds had joint efficiencies in excess of 90%; whereas the low cooling rate welds had joint efficiencies in the range of 85 to 90%. The high cooling rate welds also appear to have slightly greater strains at peak load. Filler metal strength did not have a distinguishable effect on the static tensile properties.

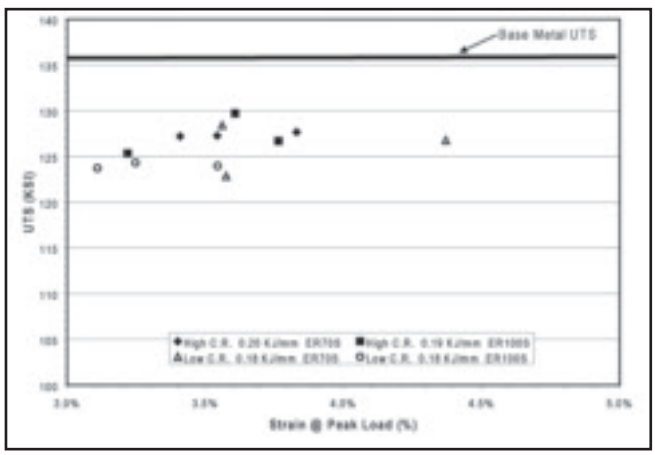

Fig. 22 — Dynamic tensile test results of TRIP 780 butt joints.

The dynamic tensile test results of the DP 780 butt joints are shown in Fig. 16. The results are presented in terms of ultimate tensile strength and the strain at peak load. All of these specimens failed in the softened region of the far HAZ. Ultimate tensile strengths ranged from 122 to 132 ksi (841 to 910 MPa), and strain at peak load ranged from 2.25% to less than 4.0%. Neither filler metal strength nor cooling rate condition had a distinguishable effect on the dynamic tensile properties of the DP 780 butt joints.

Figure 17 shows TRIP 780 lap joint static tensile results for different filler metal and cooling rate conditions. The data from Fig. 17 indicate the following:

- Joint efficiencies ranged from about 50% to about 98%. Strains at peak load ranged from less than 3% to nearly 8%.
- Specimen failure occurred either in the far HAZ (i.e., near the point of greatest softening) or at the weld fusion boundary.
- Filler metal strength had no discernable effect on the weld tensile properties.
- Welds produced under high cooling rate conditions had a significantly lower joint efficiency and strain than the welds produced under low cooling rate conditions. This difference was primarily attributed to porosity in the welds produced with the high cooling rate conditions (using short-circuit transfer).

The low cooling rate lap welds produced with the ER70S-6 welding wire failed in the softened region of the HAZ. Figure 18 shows micrographs of a low cooling rate weld produced with the ER100S-G wire, which failed along the weld interface of the top sheet. The right side of the right micrograph reveals a very small amount of porosity to be present. However, two of the low cooling rate welds produced with the ER100S-G wire failed along the weld interface of the top sheet without observable porosity.

Five of the six high cooling rate welds have joint efficiencies in the range of 50 to 78%, and strains at peak load between 2.75 and 4%. Failure in these welds may have initiated at porosity present at the weld root, with failure along the fusion boundary of the top sheet. Figure 19 shows micrographs of one of these welds. The outlying high cooling rate weld (with about 85% joint efficiency and 5.75% strain at peak load) failed along the weld interface of the bottom sheet.

Figure 20 shows the TRIP 780 lap joint dynamic tensile results for different filler metal and cooling rate conditions. As shown, ultimate tensile strengths ranged from 54 to 126 ksi (372 to 867 MPa) and strain at peak load ranged from less than 1% to over 5%. Referring to Fig. 20, the high cooling rate TRIP 780 lap joints had lower strengths and strains at peak load. These welds failed along the weld interface presumably due to porosity present at the root. All of the low cooling rate TRIP 780 lap welds produced with the ER70S-6 wire failed in far HAZ of the bottom sheet. Of the low cooling rate TRIP 780 lap joints produced with the ER100S-G wire, two dynamic tensile specimens failed in the softened region of the far HAZ, and one failed along the weld interface of the top sheet without the presence of porosity at the weld root. Analysis of Fig. 20 indicates that filler metal strength did not have a distinguishable effect on the dynamic tensile test results of the TRIP 780 lap joints.

The static tensile test results of the TRIP 780 butt joints are shown in Fig. 21. All of these welds failed in the softened region of the far HAZ with joint efficiencies in excess of 89%. On average, high cooling rate welds had higher strains at peak load than the low cooling rate welds. As was the case with the DP 780 butt joint welds and the TRIP 780 lap welds, filler metal strength did not appear to influence the static tensile properties.

Figure 22 shows the dynamic tensile test results of the TRIP 780 butt joints. All of these specimens failed in the softened region of the far HAZ. The ultimate tensile strengths of the TRIP 780 butt joints ranged from 122 to 130 ksi (841 to 896 MPa), and strain at peak load was generally between 3 and 4%. Analysis of Fig. 21 indicates that neither filler metal strength nor cooling rate condition had a distinguishable effect on the dynamic tensile test results of the TRIP 780 butt joints. It should be noted that the low cooling rate TRIP 780 butt joints had dynamic tensile properties comparable to the TRIP 780 lap joints and the DP 780 butt joints. However, on average, the TRIP 780 butt joints had slightly higher strain at peak load compared to the DP 780 butt joints.

Discussion

The chemical compositions of DP 780 and DP 980 are similar, with the latter having a higher percentage of carbon and other hardenability alloying additions. The base metal microstructure of the DP steels consists of a ferrite matrix with degenerate martensite islands, with the DP 980 having a higher proportion of martensite. The results of this project indicate that the process variables investigated have similar effects on the DP 780 and DP 980 HAZ and weld metal microstructure. This is expected when one considers that the base metal microstructure and chemistry of the two steels are similar.

The base metal microstructure of TRIP steels consists of a ferrite matrix with islands of martensite, bainite, and retained austenite. The TRIP 780 investigated in this study contains a relatively high amount of aluminum (1.8 wt-%). Aluminum is a ferrite stabilizer and (when above approximately 0.8 wt-%) can allow ferrite to remain stable at temperatures approaching the melting point of the material (Refs. 1, 3). The results of this investigation verified that retained ferrite is present in all regions of the TRIP 780 HAZ.

Because the microstructures of the DP and TRIP steels are substantially different, the results for these steels are discussed separately.

DP 780 and DP 980 Steels

Hardness traverses indicate that the weld has regions of significant hardening and softening depending on the base metal grade, filler metal type, and cooling rate conditions (as determined by welding heat input and heat sinking). The location of greatest hardening is in the near HAZ (adjacent to the fusion boundary), where the far HAZ experienced softening.

For DP 780 welded with ER70S-6 wire, the softest location in the weld is the far HAZ. Gleeble test results indicate that the DP steels both fully transform to austenite upon heating to 1000°C. The minimum hardness location corresponds to the point in the HAZ where the temperature is near the minimum required to begin forming austenite (A_{C1} boundary). This softening is probably attributable to tempering of the degenerate martensite. Mechanical testing showed that this softened region limits the DP 780 weld strength, and that a higher-strength consumable did not provide static or dynamic tensile strength improvements. During static tensile testing, cooling rate had only a slight effect on the DP 780 butt joint efficiency; for the high cooling rate condition joint efficiencies exceeded 90%, while for the low cooling rate condition joint efficiencies ranged from 85 to 90%. During dynamic tensile testing, cooling rate did not have a distinguishable effect on the strength of the DP 780 butt joint welds.

The microstructure and peak hardness of the near HAZ were strongly influenced by both cooling rate and base metal composition. A predominately martensitic microstructure is present in the region of peak hardness (395 HV) in the DP 980 high cooling rate weld, while the DP 780 had a somewhat softer (375 HV) mixture of martensite and bainite. The peak hardness of the low cooling rate DP 780 weld (260 HV) is significantly less than that of the high cooling rate DP 780 weld (375 HV). This difference in hardness is probably a result of autotempering of the martensite during the slower cooling cycle. In other words, the slower cooling rates allow martensite formed in the near HAZ sufficient time at temperatures in which tempering can occur. The potential implications of the hardness increase in the near HAZ region are not well understood.

As previously mentioned, the microstructure of both DP 780 and DP 980 consists of a ferrite matrix with degenerate martensite islands. During cold rolling of these materials, the stress and strain distribution in the two structures is different (Refs. 4, 5). The strain tends to concentrate in the soft ferrite (Ref. 4). Because DP 980 has a lower fraction of ferrite than DP 780, it may have a higher dislocation density in the ferrite phase of its microstructure. Therefore, prestrain produces a larger increase in base metal hardness for the DP 980 steel than for the DP 780 steel.

Welding on prestrained DP 780 and DP 980 resulted in a wider HAZ and the minimum HAZ hardness being slightly greater than that of the welds without prestrain. In addition, it was observed that for each respective material the high cooling rate weldment had a slightly greater minimum HAZ hardness than the low cooling rate welds with nominally the same amount of prestrain. The differences in the HAZ of the welds produced with prestrain to those produced on the as-received base metal are attributable to the process of recovery. For both DP grades, the minimum HAZ hardness of the prestrained weld remains greater than that of the weld without prestrain, which is likely due to the weld thermal cycle in the far HAZ being insufficient for completion of the recovery process. Compared to DP 780, a greater reduction in base metal hardness occurs in the HAZ of prestained DP 980. This may be due to the higher dislocation density present in the ferrite phase of this material producing a larger driving force for recovery.

Based on the fusion zone data presented in the tables, weld metal microstructure and hardness appear to be predominately influenced by the cooling rate, rather than the DP grade. Welds on DP 780 produced using both wires tended to consist of predominately acicular ferrite with varying degrees of bainite and martensite. The welds on the DP 780 and DP 980 produced using the ER70S-6 wire had similar microstructures and hardness, and no correlation could be made between base metal dilution and microstructure. Analysis of the microstructure and the resulting fusion zone hardness indicates that dilution of the filler metal by the base metal does play a role in weld metal microstructure evolution, although the effect of dilution was more pronounced for the TRIP 780, which is discussed later.

When the DP 980 was welded with the ER70S-6 consumable, the lowest hardness occurred in the fusion zone. This suggests that a higher-strength electrode would be required to avoid undermatched weld metal strength and consequent failure through the fusion zone. Application of a higher-strength electrode may be required to shift the failure location to the softened region of the HAZ.

TRIP 780 Steel

The TRIP 780 welds had a continuous structure of ferrite grains along the fusion boundary. The presence of ferrite along the fusion boundary can be explained with the equilibrium phase diagram shown in Fig. 12. For TRIP 780, at temperatures near the liquidus, ferrite is the only thermodynamically stable phase.

For all locations within the TRIP 780 HAZ, the fraction of ferrite in the microstructure is greater for the welds produced with low cooling rate compared to high cooling rate. The microstructure of the low cooling rate weld at the point of peak HAZ hardness consists of predominately ferrite grains separated by regions of degenerate martensite. As previously noted, the term degenerate martensite is used to describe regions that appear to be martensite at optical microscopy levels, but may contain tempered martensite and/or bainite constituents. The microstructure in the high cooling rate weld at the location of peak HAZ hardness consists of a mixture of martensite and large ferrite grains. In both cases, the fraction of ferrite in the HAZ microstructure increases from the point of peak HAZ hardness to the location of minimum HAZ hardness. The microstructure of the high cooling rate weld has greater hardness at each HAZ location between the points of minimum and peak hardness.

The microstructure evolution in the HAZ of TRIP steels can be separated into two different regions. The regions that heated above the A_{C1} temperature (700°C) and the regions heated below the A_{C1} temperature.

Referring to Fig. 12, the regions heated above the A_{C1} do not entirely transform to austenite due to increased stability of ferrite. As a result, the regions heated above the A_{C1} will remain in a two-phase (austenite + ferrite) region throughout the heating cycle. Depending upon the peak temperature, the ferrite fraction may increase from the original level. This often resulted in a continuous necklace of ferrite along the weld interface of the welds produced on the TRIP 780 steel. Similar microstructural observations have been noted for multipass self-shielded gas metal arc welds (Refs. 6, 7). As the HAZ starts cooling, a small fraction of the austenite may be retained, but the larger fraction decomposes into either bainite or martensite. The rate of cooling will determine the nature of this microstructure mixture. This is supported by the HAZ microstructure of welds made with both the nominally high and low cooling rate conditions.

The regions heated below the A_{C1} (far HAZ) and cooled are expected to undergo subtle microstructural changes. As previously noted the base metal microstructure of TRIP steel consists of a ferrite matrix with islands of martensite, bainite, and retained austenite. Depending upon the peak temperature, the retained austenite may transform to martensite upon cooling; this can only be determined using transmission electron microscopy. At a given location of the far HAZ, the martensite formed from the retained austenite, as well as that present in the as-received base material, may undergo tempering. The degree of martensite tempering is dependent on the weld thermal cycle at the given location. Based on the measured hardness of the welds produced with both cooling rate conditions, lesser degrees of martensite tempering is expected in the welds made with the high cooling rate condition. The extent of softening appears to decrease with an increase in distance from the A_{C1} boundary.

Prestrain had a more pronounced effect on the TRIP 780 than was observed with the DP steels. During deformation of TRIP steels at ambient temperatures the retained (quasi-stable) austenite progressively transforms into martensite as the material is strained (Refs. 4, 8). Therefore, the increased base metal hardness is due to both the new martensite formed, and an increase in the dislocation density of the ferrite grains. For both cooling rate conditions, prestrain did not increase the peak HAZ hardness, but did increase the hardness in the region between the A_{C1} boundary and the peak HAZ hardness location. In addition, the minimum HAZ hardness of the welds made on the prestrained base metal remained greater than the hardness of the as-received base metal.

Welds produced on TRIP 780 with the ER70S-6 wire consisted primarily of bainite with a small fraction of acicular ferrite. Compared to the DP 780 welds, for each condition of joint geometry and cooling rate these welds tended to have slightly higher hardness. When the ER100S-G wire was used, the microstructure of the TRIP 780 welds tended to consist either of martensite and/or bainite. For this electrode/base material combination, acicular ferrite was only observed in the microstructure of the low cooling rate lap joint weld. Compared to the DP 780 welds produced with the ER100S-G wire, for each condition of joint geometry and cooling rate the TRIP 780 welds had significantly higher hardness.

The fusion zone hardness data suggest that base metal dilution has a greater effect on weld metal hardenability for TRIP 780 than for DP 780 or DP 980. Of the three materials, TRIP 780 appears to be the most heavily alloyed (Table 2). Table 15 lists the carbon equivalents of these materials, which were calculated using the formula proposed by Yurioka et al. (Ref. 9). As listed, TRIP 780 has the highest carbon equivalent. However, it is important to note that the carbon equivalency formula does not consider aluminum. In this regard, the major effect of dilution is attributed to higher carbon content in TRIP steels. As Kou reported, increasing the alloying content of weld metal increases its hardenability by pushing the nose of the continuous cooling transformation curves to longer times (Ref. 10). Thus, harder constituents such as bainite and martensite are more likely to form in the welds produced on TRIP 780.

A wide range of joint efficiencies (50 to 90%) and ultimate tensile strengths (54 to 128 ksi) were obtained for the TRIP 780 lap welds during static and dynamic testing, respectively. Failure was either along the weld interface or more commonly in the softened region of the HAZ. Five of the six TRIP 780 lap welds produced with high cooling rate conditions failed along the weld interface during static testing (presumably due to porosity at the weld root) at significantly lower strength and ductility than the welds produced with low cooling rate conditions. Notably, some of the welds failed along the weld interface without any indication that porosity was present at the weld root. As mentioned previously, the weld interface of the TRIP 780 welds contains a continuous region of large ferrite grains. This region most likely

has lower strength than the surrounding weld metal and HAZ microstructure. The weld root and any porosity present near the root serve as stress concentrations. Fracture can initiate at these stress concentrations and propagate through the lower-strength ferrite grains along the weld interface. Butt joint welds that lacked such stress concentrations all failed in the softened region of the HAZ at joint efficiencies of over 90% (static testing) and ultimate tensile strengths between 122 and 130 ksi (dynamic testing). For the butt joints that underwent static tensile testing, higher cooling rate conditions tended to increase the joint efficiency slightly. However, cooling rate conditions did not have a distinguishable effect on joint strength during dynamic tensile testing.

For each condition of cooling rate and joint geometry, filler metal strength did not have a distinguishable effect on either joint strength or ductility. Filler metal strength may play a larger role in static strength for prestrained TRIP 780. Prestraining increased the hardness of the softest point in the HAZ, which may shift the failure to the fusion zone. It is possible, however, that the continuous ferrite band along the fusion boundary may be the point of failure on prestrained material, regardless of the filler metal strength. Additional work is needed to assess the effect of prestrain and the continuous ferrite band on weld tensile properties.

Summary and Conclusions

This work primarily investigated the effects of cooling rate (welding heat input and fixture heat-sinking), prestrain, filler metal selection, dilution, and postbaking on the microstructure and mechanical properties of GMA welds on coated DP 780 and TRIP 780 sheet metal lap joints and butt joints. A limited amount of testing was also conducted for DP 980 lap joints. The most significant conclusions are listed below.

1) The DP steels showed varying degrees of HAZ hardening and softening depending on the material grade, prestrain, and cooling rate condition. The relatively high aluminum content of the TRIP 780 steel allowed retained ferrite to be present in all regions of the HAZ, along with a continuous region of coarse ferrite along the weld interface. This resulted in the TRIP 780 having lower peak HAZ hardness than the DP 780.

2) Fusion zone microstructure and hardness were found to be affected by the base metal chemistry, the cooling rate condition, and the filler metal composition.

3) Filler metal strength did not affect the static or dynamic tensile properties of either the TRIP 780 lap or butt joint welds, or the DP 780 butt joint welds. All of the TRIP 780 and DP 780 butt joints failed in the soft HAZ. The results of the lap joint tests showed a greater variation in strength that is primarily attributed to porosity at the root of the weld.

4) Additional work is needed to relate HAZ and fusion zone microstructures, hardness profiles, and geometric discontinuities to fatigue, bend, impact, and crush performance. In particular, work is needed to evaluate the effect that the ferrite region along the fusion boundary has on the mechanical properties of TRIP 780 lap joints.

References

1. Biro, E., and Lee, A. 2004. Welded properties of various DP600 chemistries. *Proc. Sheet Metal Welding Conference XI*, Sterling Heights, Mich.

2. Gould, J. 2007. Interview. Edison Welding Institute. Columbus, Ohio.

3. Sundman, B., Jansson, B., and Anderson, J. O. 1985. The thermo-calc databank system. *Calphad* 9 (2): 1–153.

4. Hulka, K. 2005. Dual phase and TRIP steels. *www.us.cbmm.com.br/english/sources/techlib/info/dualph/dualphas.htm.*

5. Hsu, C., Soltis, P., Barton, D., and Occhialini, C. 2004. Weldability of dual-phase steel with arc welding processes. *Proc. Sheet Metal Welding Conference XI*, Sterling Heights, Mich.

6. Babu, S. S., David, S., and Quintana, M. 2001. Modeling microstructure development in self-shielded flux cored arc welds. *Welding Journal* 80 (4): 91-s to 97-s.

7. Quintana, M., Mclane, J., Babu, S. S., and David, S. 2001. Inclusion formation in self-shielded flux cored arc welds. *Welding Journal* 80(4): 98-s to 105-s.

8. Senuma, T. 2001. Physical metallurgy of modern high strength steel sheets. *ISIJ International* 41(6): 520–532.

9. Yurioka, N., Suzuki, H., Ohshita, S., and Saito, S. 1983. Determination of necessary preheating temperature in steel welding. *Welding Journal* 62(6): 147–153.

10. Kou, S. 2003. *Welding Metallurgy,* Second Edition. Hoboken, N.J.: John Wiley & Sons, Inc.

11. Farrar, R. A., and Harrison, P. L. 1987. Acicular ferrite in carbon-manganese weld metals: An overview. *Journal of Material Science* 22: 3812–3820.

12. Abson, D. J., and Pargeter, R. J. 1986. Factors influencing as-deposited strength, microstructure, and toughness of manual metal arc welds suitable for C-Mn steel fabrications. *International Metals Review* 31(4): 141–194.

13. Babu, S. S., and Bhadeshia, H. K. D. H. 1991. Mechanism of the transition from bainite to acicular ferrite. *Materials Transactions*, JIM, 32(8): 679–688.

14. Bode, R., Meurer, M., Schaumann, T. W., and Warnecke, W. 2004. Selection and use of coated advanced high-strength steels for automotive applications. *Proc. Galvatech '04 Conference*. Association for Iron & Steel Technology, Warrendale, Pa.

15. Shaw, J. R., and Zuidema, B. K. 2001. New high strength steels help automakers reach future goals for safety, affordability, fuel efficiency and environmental tesponsibility. *Journal of Materials and Manufacturing* 5(110): 976–983.

16. Lippold, J. 2004. *Welding Metallurgy Principles*. National Excellence in Materials Joining Education and Training. Columbus, Ohio.

17. Wagner, R. *Ferrous Metallurgy.* The Ohio State University Materials Science & Engineering. Columbus, Ohio.